Next Materials 12 (2026) 102415

Contents lists available at ScienceDirect

Next Materials

journal homepage: www.sciencedirect.com/journal/next-materials

Research article

Intrinsic superconductivity and correlations in stoichiometric materials without external perturbations

Shermane M. Benjamin

The National High Magnetic Field Laboratory, 1800 E. Paul Dirac Drive Tallahassee, FL 32310, USA

ARTICLE INFO

Keywords:
Superconductivity
Electrostatics
Energy density
DFT
STP pressure
Ideal gas law
Empirical
T_c

ABSTRACT

Estimating the chemical and physical properties that govern the emergence of superconductivity remains a central challenge in condensed matter physics, in part because a universal indicator/descriptor analogous to band structure does not yet exist. Historically, simple empirical relations, such as the Wiedemann-Franz law first described in 1853, linked seemingly disparate phenomena like thermal and electrical conductivities in metals long before a comprehensive theoretical understanding was established. Regarding superconductivity, in this work, we introduce a phenomenological real-space approach grounded in local potential energy calculations that uses only elemental composition and atomic positions to partition superconductors from non-superconductors. These inputs are also used in Density Functional Theory (DFT), but our method eliminates the need for complex reciprocal-space computations or empirical fitting. By systematically analyzing electrostatic interactions within repeated bond units in relation to unit cell volumes, our strategy yields a discrete, integer-based classification that reliably distinguishes superconductors from non-superconductors with high accuracy. This computationally efficient and physically transparent framework offers a robust alternative to traditional approaches and provides a fresh electrostatic perspective on superconductivity. This study prioritizes a data-centric methodology to drive superconductor discovery. It is formulated in the spirit of historical empirical rules (e.g., the Wiedemann-Franz relation metals) and does not aim to affirm or dispute BCS theory.

1. Introduction

Empirical rules and phenomenological correlations have long been an integral part of research regarding electrical conductivity, providing practical guidance long before complete microscopic explanations were developed [1–5]. A canonical example is the Wiedemann-Franz law [6]. It was first observed as an empirical proportionality between electronic thermal and electrical conductivities in metals; an observation which helped distinguish metallic from non-metallic behavior well before a full quantum transport description was established [7]. Similarly, regarding superconductivity, Bernd Matthias's valence-count heuristics emerged from systematic experimental observations [8–12]. His results were later organized into a large body of superconductivity data to be used as a compact guideline towards new superconductors before the establishment of BCS theory. To date, Matthias' ideas regarding valence electron-count is still being explored in systems like high-entropy-alloys [13], for example, where chemical composition and complexity are shown to strongly effect superconducting properties like T_c. These precedents illustrate that concise, experimentally motivated relations can both summarize complex trends and motivate deeper theoretical work. In fact, current state-of-the-art approaches like machine-learning [14–17] also search for correlations among experimental data to predict superconductivity in elements and known materials. However, ultimately, predictions are made in this method without explicitly revealing underlying material-dependent functions for simpler computational predictions [18].

In this report, we propose a simple empirical formula based on **local potential** calculations to estimate the emergence of superconductivity. We introduce a new empirical indicator, the **Coulomb bond energy density** (CBED), defined for a crystal purely from atomic identities, element coordinates, and unit structure. In essence, CBED is computed by summing over pairwise **local interactions** between electrons of central atoms and the effective nuclear charge of nearest-neighboring atoms in bond units, then dividing by the unit cell volume. It is a local electrostatic potential energy density that measures how strongly electrons are bound in their local chemical environment. This is an energy scale that plausibly affects the local propensity for electron pairing. We find that the structure-based criterion developed for CBED robustly discriminates superconductors from non-superconductors with high accuracy in elemental solids, with preliminary results on multi-component compounds reported as well. Note, only compounds existing at standard pressure are examined in this study.

E-mail address: benjamin@magnet.fsu.edu.

https://doi.org/10.1016/j.nxmate.2026.102415
Received 16 March 2026; Received in revised form 23 May 2026; Accepted 1 June 2026
Available online 10 June 2026

Table 1
Key indicators for superconductivity emergence.

Prediction	β	α
Superconductivity **likely** to emerge when **both conditions** are met…	≥ **11**	*integer* (between 2 and 9 [±0.12]) **OR** 1.27 [+0.09 , −0.1]

2. Predicting superconductivity in elements

Six experimental parameters (i.e., material properties) are used to calculate the CBED (Eq. (1)) of repeating chemical bond units in stoichiometric compounds. A chemical bond unit in a crystalline solid is the smallest repeating chemical unit that contains enough atoms and explicit nearest neighbor bonding relationships to reconstruct the entire solid by spatial repetition. This unit reflects both the chemical composition of the material and the coordination of atoms with their nearest neighbors, the primary bonds that define the local bonding environment. Within a repeating bond unit, first, the total Coulomb energy of all chemical bonds connecting a central atom to its outer atoms, $E_{\text{Coul.}}$ (Eq. (2)), is calculated. The energy is then divided by the number of central atoms N_A (i.e., = 1 for elements) and the unit cell volume V_{unit}. All variables can be easily extracted from freely available C.I.F. data and cataloged peer-reviewed data, [19–21] and the periodic table of elements. All C.I.F. data were obtained from the same open data source location, materialsproject.com [19]. $E_{\text{Coul.}}$ is a function of the number of outer electrons N (s+d for transition metals) of the center atom, screened nuclear charge Z_{eff} (2nd smallest tabulated) of a distant outer atom, [20,21] the bond length L between N and Z_{eff}, number of these specific bonds N_B, elementary charge e, and Coulomb's constant κ.

$$\text{CBED} = \frac{E_{\text{Coul.}}}{N_A V_{\text{unit}}} \tag{1}$$

Essentially, Eq. (2) accounts for the effective/screened Coulomb interactions often considered when aiming to predict superconducting properties of compounds [22–29]. For our model, it is the real space representation of the effective potential for a charged particle of size $N_x \cdot e$ at the center of a bond-unit. To this end, Eq. (1) is used to examine the correlation between this energy scale relevant to superconductivity and the unit cell volume.

$$E_{\text{Coul.}} = \frac{N_B N_x Z_x (e^2 \kappa)}{L} \tag{2}$$

A schematic for three example solids displaying the six experimental parameters needed for CBED is shown in Fig. 1. A fictious elemental "X" in Fig. 1.A is used to map out each variable. Examples of repeating bond units of solid elemental copper (Fig. 1.B) and MgB_2 (Fig. 1.C) are also depicted.

When Eq. (1) is calculated for single-element compounds, superconductors and non-superconductors separate into two categories with 74% accuracy. To see the partitioning, We express CBED in normalized scientific-notation form, CBED = $C_0(\alpha \cdot 10^{\beta})$, with C_0 = 7.3 Pa chosen as the reference energy density scale because it centers the mantissa distribution for the complete elemental census; this choice is algorithmically determined and robust to modest variations in C_0 (Figure S1). The reparameterization of CBED is shown in Eq. (3). Remarkably, most superconducting elements appear at $\beta \geq 11$ (evident in top table of Fig. 2) and α = integer (between 2 and 9 [±0.12]) or α = 1.27 [+0.09, −0.10] (evident in bottom table of Fig. 2), where brackets represent observed errors in for maximum separation in sorting. This analysis is summarized in Table 1. Lithium is the only elemental superconductor with β=10; its T_c is ~0.4 mK. Also notice that although the physical meaning of α is unclear, it seems to be related to an element's outer orbital as shown in Fig. 2's top table. We arrive at this conclusion since exactly 80% of s-elements, 68% of p-elements, and 93% of d-elements are clearly differentiated by β = 10, 11, and 12, respectively.

$$\text{CBED} = (\mathbf{7.3\ Pa})(\alpha \cdot 10^{\beta}) \tag{3}$$

There are several important things to keep in mind about the predictive power of Eq. (3) for elements. These points are visually illustrated in Fig. 2 where blue squares represent superconductors and red squares are nonsuperconductors. With aforementioned simultaneous constraints on α and β, CBED predicts the total number of superconductors (prediction=24/61, actual=23/61) and the portion of superconductors in each orbital group (s: prediction=actual=2/10, p: prediction=actual=6/22, d: prediction=16, actual=15) with near perfect accuracy.

Incorrect predictions, shown with white dots in bottom table of Fig. 2, occur at the boundary between superconductors and non-superconductors. This point is illustrated clearly for s-elements and p-elements. Even so, high prediction accuracy means the general location of superconducting elements are predicted well. For instance, the upper s-block and the lower left corner of the p-block are predicted to be superconducting. Most heavy d-elements (>Zn) are predicted to superconduct as well, where row n=4, which contains light d-elements, is sorted with 88% accuracy.

Statistically, with previously defined "integer-like" values of α ($\beta \geq 11$), we find 16 of 24 superconducting elements versus 7 of 37 non-superconducting elements satisfy this condition. The Pearson chi-square test yields $\chi^2 \approx 14.17$ and $p \approx 0.00016$, firmly rejecting the null hypothesis of no relationship between superconductivity and integer-like α values. The odds ratio of 8.6 (95% CI: 2.6–27.8) quantifies a strong association, while the difference in proportions (66.7% vs. 18.9%) of 47.8 pp (95% CI: 25.1–70.5) highlights both statistical and practical significance. Keep in mind, this analysis is conducted on a complete dataset since all stable elements are known to date.

3. Preliminary study on 84 selected multicomponent compounds

This section applies the CBED indicator and the summarized guideline (Table 1) to a representative, non-exhaustive set of eighty-four binary and higher-order compounds selected to demonstrate the method's applicability. Given the large number of existing complex compounds, the reported statistics are intended to be illustrative rather than exhaustive, and no formal statistical tests (p-values) are included. Formal hypothesis testing is omitted because the dataset is illustrative and does not sample the full space of known compounds; comprehensive statistical inference is therefore deferred to future large-scale studies. Details of the data selection procedure are provided in supplementary Figure S2. For consistency, the categories shown in Fig. 2 (well-known compounds, tellurides, selenides, and sulfides) begin with simple binaries (AB) and subsequently expanded to include structural and chemical analogs (e.g., FeSe → NiSe). Binaries with progressively larger chalcogen content (2–8 chalcogens per formula unit) and selected bulk ternary chalcogenides are also shown. The dataset primarily emphasizes stoichiometric compounds with related chemistry and structure, allowing observed trends to reflect underlying structural and chemical variation rather than artifacts of sampling.

Unlike elements, $N_A \geq 2$ for binaries and more complex compounds since the CBED averages the total Coulomb energy $E_{\text{Coul.}}$ over the number of central atoms per bond unit. For example, N_A = 2 for $ZrSe_2$ and

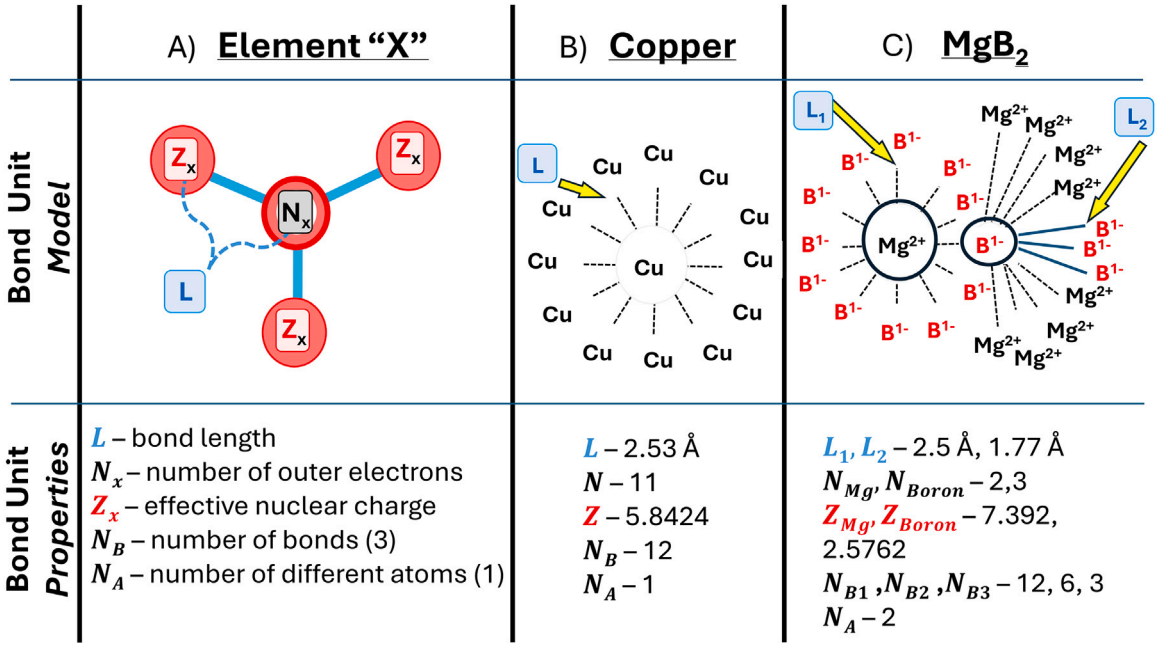

Fig. 1. Bond unit of three solids (not drawn to scale). (A) Stick-and-ball model for a bond unit of fictitious element "X". Variables L, N, Z_{eff}, N_B, and N_A are indicated. Variables are quantified for bond units of (B) solid elemental copper and (C) solid MgB_2. The latter illustrated bond unit repeats to ultimately form MgB_2's unique hexagonal (P6/mmm) bulk structure. According to accepted C.I.F. data [19], Mg^{2+} is bonded to twelve equivalent B^{1-} atoms and B^{1-} is bonded to six equivalent Mg^{2+} atoms and three equivalent B^{1-} atoms. All Mg-B bonds (dashed lines) are 2.50 Å. All B-B bonds (solid blue lines) are 1.77 Å.

$N_A = 4$ for $ZrTe_3$. To this end, the CBED output successfully identifies the superconducting compounds shown in Fig. 3 with high accuracy across a range of mechanisms. Notably, CBED singles out MgB_2 as the only superconductor among seven diborides (MB_2 [M = Mg, Mo, W, Al, Zr, Tl, and Hf]) with $\alpha = 5.04$ and $\beta = 11$, and it distinguishes the unconventional superconductor Sr_2RuO_4 ($\alpha = 2.08$ and $\beta = 11$) from the structurally analogous Sr_2RhO_4. Iron-based superconductors such as FeSe and FeS are likewise separated from structurally and stoichiometrically similar analogs. On this selected dataset of complex compounds, CBED attains roughly 80% classification accuracy, but there are notable failure modes: for example, Chevrel phase materials MMo_6S_8 (M = Pb, Sn, Tl, and In) are poorly classified (≈40% accuracy; see lower right of Fig. 3). These exceptions highlight the limits of the present nearest-neighbor, stoichiometric formulation and motivate targeted follow-up work on the chemistries that produce systematic misclassifications.

4. T_c's dependence on α in elemental superconductors

Having established α and β as sufficient variables for flagging superconducting behavior, we now examine α's empirical correlation with T_c across elemental solids. While our primary aim is to determine whether a material is likely to exhibit superconductivity, the potential to gain insight into its T_c, even qualitatively, would offer added predictive power. In this context, we define a reference quantity, T_{c-max}, as the maximum reported transition temperature for each element and evaluate how this quantity varies with α.

As shown in Fig. 4, T_{c-max} exhibits pronounced local maxima near α = 1, 6, and between 4 and 5. This trend suggests that higher elemental superconducting temperatures may occur preferentially at specific values of α. Interestingly, Matthias found the same qualitative features [8] in T_c versus the average valence electrons-count (e) per atom (a). He showed that transition temperatures peaked near e/a= 4.5 and 7. While similar on the surface, differences related to inputs and scope are essential to emphasize. Matthias rules rely on d-electron behavior which is only applicable to transition metals and a few intermetallic compounds consisting of non-transition metals. The relation e/a for non-transition metals does not exhibit oscillatory behavior and requires a separate formulism for analysis; therefore, a peak at e/a < 2 is possible to observe, unlike α=1.27 in our study. The other crucial difference is that superconductors appear at integer-like values of α and it is unitless, as opposed to continuous values for e/a, within similar ranges.

An application to calculate α and β in* Eq. (3) *for ordered solids with up to four central atoms is available upon request and will be freely accessible online.

5. Preliminary results on T_c's dependence on α in multicomponent superconductors

The T_{c-max} of multicomponent superconductors listed in this report are plotted against α as shown in Fig. 5. Remarkably, MgB_2, known for its anomalously high T_c among binaries, has an α value of 5.04 (β=11), falling directly within one of these peak regions similar to elements. Though the list of compounds is not comprehensive, it contains the only stoichiometric binary that is known to have the highest T_c, MgB_2. Similarly, the structurally analogous high pressure superconducting phase, WB_2, has a calculated α at 1.26 (a local maxima in Fig. 5, guided by the dashed line) with β=11. The binary MoB_2 is also similar in structure to MgB_2, however, CBED incorrectly predicts it to not be a superconductor since β=10.

6. Limitations and accuracy

While the empirical framework developed here initiates a way to distinguish superconductors from non-superconductors using only real-space quantities, it necessarily involves simplifying assumptions and exclusions. These limitations arise from (1) practical considerations, such as data availability and opportunity cost, and (2) conceptual constraints inherent to the model and its underlying assumptions. The following points summarize several constraints of our CBED approach. While these limitations may be addressed in future work, they are beyond the scope of this report.

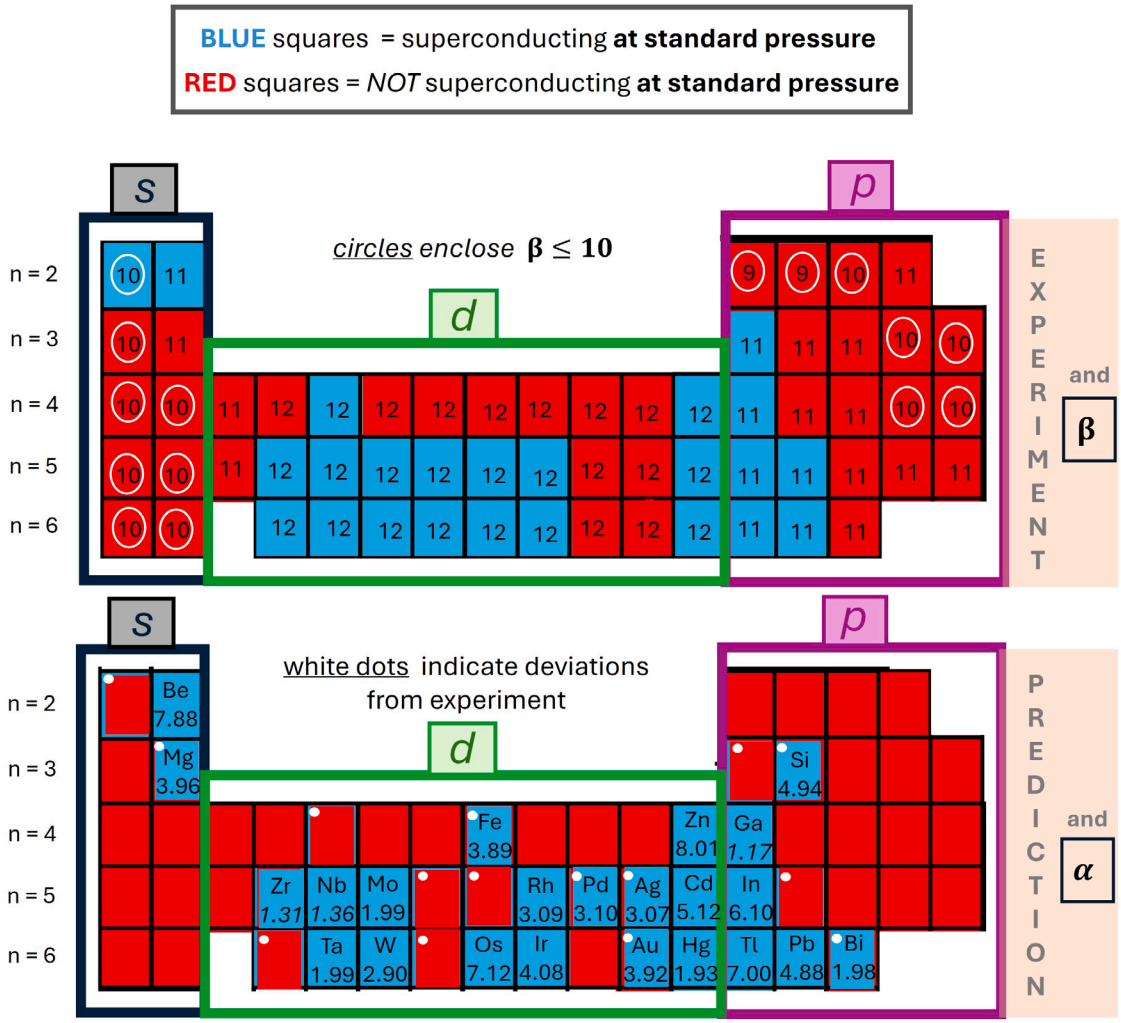

Fig. 2. Periodic Tables of Elements at standard pressure. Top table illustrates the location of **experimentally verified** superconductors (Blue) and non-superconductors (Red) along with β calculated from Eq. (3). White circles indicate $\beta \leq 10$. Bottom table illustrates the location of **predicted** superconductors (Blue) and non-superconductors (Red), along with α calculated from Eq. (3) for elements predicted to be superconductors. White dots indicate deviations from experimental data shown in the top table. The s-block, p-block, and d-block in each table are emphasized and outlined in thick black, green, and purple borders, respectively.

(1) **Only Stoichiometric Compounds at STP:** The present analysis is restricted to compounds with well-defined stoichiometries and minimal atomic disorder. This constraint ensures that the calculated Coulomb bond energies and related quantities reflect intrinsic properties rather than extrinsic effects arising from vacancies, interstitials, or site disorder. Non-stoichiometric systems, including doped or highly defective compounds, are excluded because their local potential and carrier concentrations are not uniquely defined, rendering direct comparison unreliable. The emergence of superconductivity in these compounds are actively being explored where a different empirical rule was discovered [30–32]. Pressurized compounds have all the defined parameters of interest (unit cell volume, bond length, etc.), however, these C.I.F. parameters are mostly unreported for elevated pressures.

(2) **Exclusion of f-Block Elements:** Compounds containing lanthanide elements were excluded because their localized 4f electrons (i.e., relativistic effects) and strong magnetic moments introduce interactions that are not explicitly accounted for in our model. Magnetic fluctuations and f-electron hybridization can significantly modify superconducting behavior, often competing with pairing interactions [33]. The present empirical method fails in over 90% of lanthanide-containing cases, highlighting that a dedicated treatment of magnetism and correlated f-electrons is likely required to achieve predictive accuracy in this class of materials. Actinide-containing systems were not considered for similar reasons to Lanthanides, but also due to the lack of reliable tabulated effective nuclear charge values for their outer orbitals.

(3) **Disregarded Longer-Range and Higher-Order Interactions:** The current formulation considers only nearest-neighbor Coulomb interactions within well-defined bond units. Effects arising from next-nearest-neighbor coupling, long-range electrostatics, or multi-center bonding are not included. While CBED captures the dominant contributions to the local potential energy, these neglected interactions could play a non-negligible role in materials with extended bonding networks, delocalized orbitals, or anisotropic charge distributions. Incorporating such effects may refine predictive accuracy in future iterations of the model.

(4) **Data source and accuracy:** All input data are taken from standard sources. We parse CIF files (the IUCr-endorsed standard format for crystal structures) to get atomic positions and bond lengths and use the periodic table for element properties. Because CIFs and the periodic table are universally standardized, the correctness of the method depends only on those inputs. We do not introduce arbitrary tuning parameters requiring further interpretation.

(5) **Correlation between CBED and T_c:** Unlike similar empirical relationships explicitly involving T_c and its prediction, [30–32] the

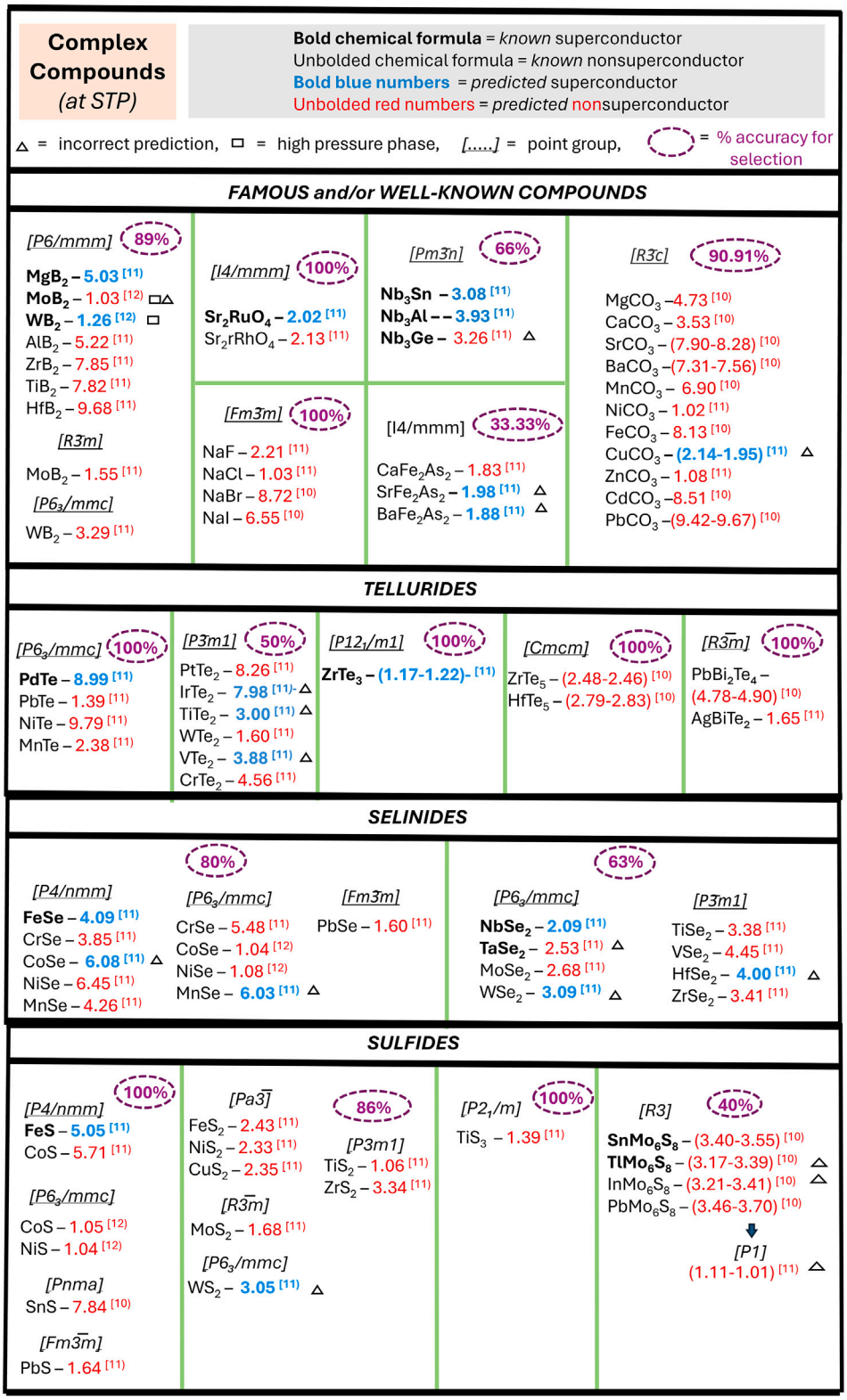

Fig. 3. Pictorial list of eighty-four known complex compounds.
The list contains four groups of representative materials: well-known examples, tellurides, selenides, and sulfides. Each compound is listed with its calculated alpha and beta values noted as $\alpha^{(\beta)}$. Bold chemical formula = known superconductor. Unbolded chemical formula = known nonsuperconductor. Blue numbers = predicted superconductor. Red numbers = predicted nonsuperconductor. Triangles = incorrect prediction. [....] = point group. Dotted circles enclose percent accuracy in sorting groups of similar stoichiometry and structure.

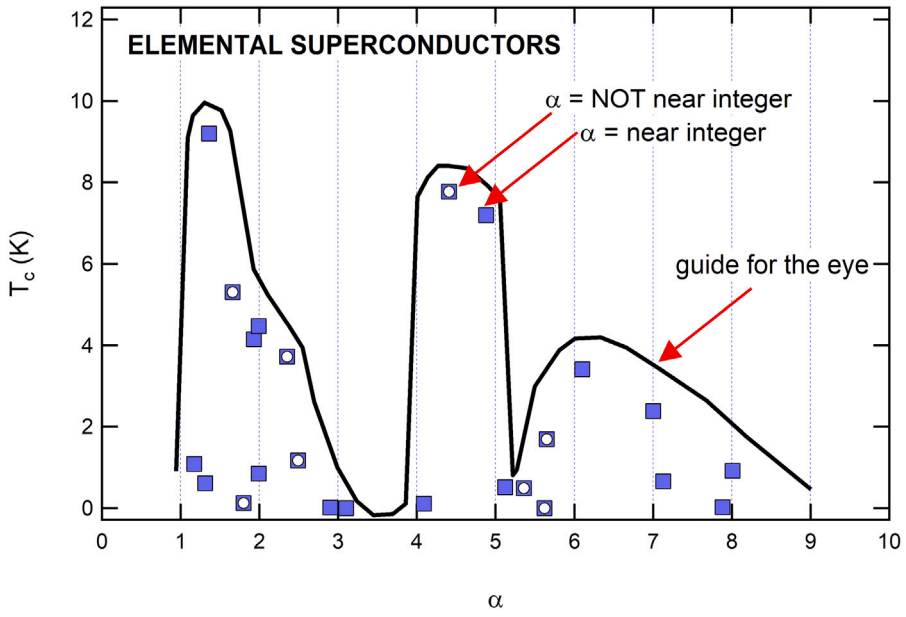

Fig. 4. T_c vs.α of elemental superconductors at STP.
Blue squares represent near integer α. Blue squares with white circles represent α outside of integer boundary. The black line is a guide for the eye for the maximum transition temperature as a function of α, $T_{c\text{-max}}(\alpha)$, in elements at standard pressure, set slightly above $T_{c\text{-max}}$ to reduce visual clutter. The transition temperature reaches a maximum near α = 1.27 (+0.09, −0.1), 5 (±0.12), and 6 (±0.12).

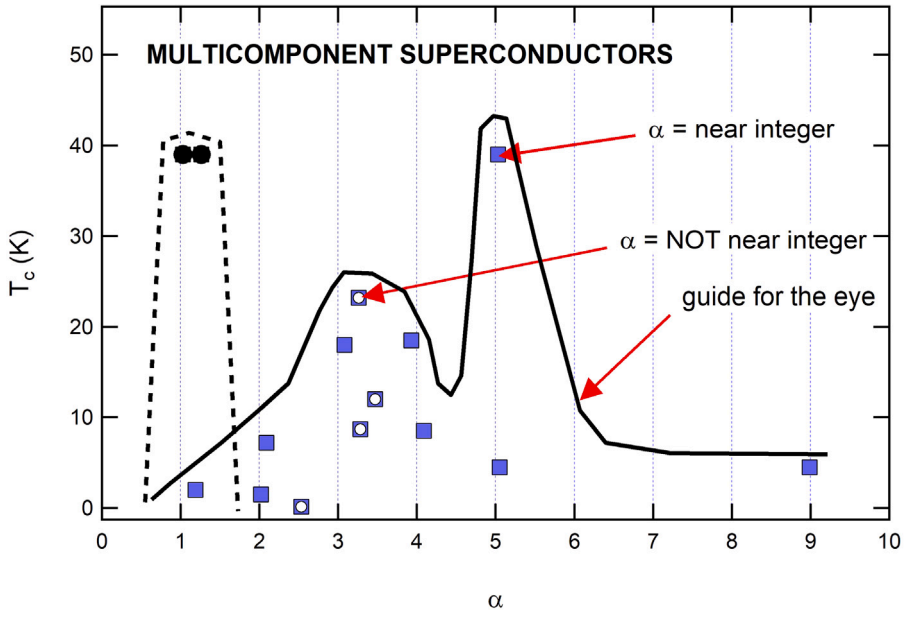

Fig. 5. T_c vs.α of multicomponent superconductors.
Blue squares represent near integer α for compounds at STP. Blue squares with white circles represent α outside of integer boundary for compounds at STP. Black circles represent near integer α for compounds at high pressure. The solid and dashed black lines is a guide for the eye for the maximum transition temperature as a function of α, $T_{c\text{-max}}(\alpha)$, in elements at STP and elevated pressure, respectively, set slightly above $T_{c\text{-max}}$ to reduce visual clutter. The transition temperature reaches a maximum near α = 1.27 (+0.09, −0.1), 5 (±0.12), and 6 (±0.12).

CBED does not linearly correlate to T_c. Efforts are underway exploring techniques used in prior studies [30] to search for quantitative and predictive linear correlations between CBED and T_c.

7. Discussion

A line of phenomenological work links the accessible free volume for conduction electrons and absolute-rate (activated-process) concepts to changes in transport and superconducting behavior. It is conceptually based on the absolute-rate theory of chemical kinetics, [34] which expresses rates in terms of an activation free energy and an attempt frequency. More recent studies have combined Eyring-style rate arguments with a free-volume picture of electronic mobility to derive phenomenological conductivity relations and to rationalize dome-like Tc trends as functions of doping or pressure [35–37]. High pressure superconductivity studies likewise emphasize structural packing and electronic free volume, often parameterized via Wigner-Seitz radii or related volume metrics, as key variables that correlate with pressure-induced changes in Tc [38].

The CBED indicator introduced here shares with these approaches an explicit sensitivity to structural packing through its normalization by unit-cell volume: decreasing unit-cell volume raises the local Coulomb energy density in CBED in a manner that is, at a phenomenological level, consistent with reduced free volume restricting electronic phase space in rate-process pictures. Mechanistically, however, the two viewpoints are distinct. Free-volume + Eyring models adopt a kinetic or mobility-based interpretation (how structural constraints affect activated processes, diffusion, or rearrangement rates), whereas CBED is an electrostatic energy-density descriptor computed from summed local Coulomb interactions within bond units and scaled by cell volume. Thus, unit-cell volume enters both descriptions but with different physical content: CBED quantifies an energetic (potential-energy) constraint on electronic states, while free-volume/Eyring frameworks quantify how structural packing governs dynamical possibilities for electronic motion.

These complementary perspectives suggest a productive pathway for follow-up work. A direct quantitative comparison between CBED and free-volume metrics (for example, Wigner-Seitz radius or normalized atomic packing fraction) across representative materials may clarify where energetic and kinetic descriptors align and where they diverge and could help identify classes of materials for which one viewpoint is more predictive. Reconciling or combining energetic (CBED) and kinetic (free-volume/Eyring) descriptors may therefore yield a richer, multi-scale framework for understanding and predicting structural influences on superconducting behavior.

8. Conclusion

In summary, our real-space Coulomb bond energy-unit volume framework establishes a widely applicable, computationally light paradigm for predicting superconductivity in well-ordered compounds. Upon evaluating the correlation CBED = ($\mathbf{7.3\ Pa}$)($\alpha \cdot 10^{\beta}$) on over 100 compounds and elements combined, we find superconductivity tends to emerge in compounds containing no f-elements when α is near an integer (or 1.27) and $\beta \geq 11$, simultaneously.

By distilling complex electronic and structural interactions into a physically transparent phenomenological indicator, our method bypasses the need for momentum-space calculations. This approach not only reproduces classical empirical observations reminiscent of Matthias's valence electron peaks but also reliably flags compounds for latent superconducting behavior. In addition, the CBED indicator's explicit dependence on V_{unit} links naturally to phenomenological free-volume and activated-process (Eyring-type) pictures: whereas free-volume/Eyring frameworks emphasize kinetic or mobility constraints, CBED quantifies a local electrostatic energy density. These complementary perspectives may be reconciled to give a richer, multi-scale understanding of structural effects on T_c. Building on earlier empirical studies [30–32] which examined concentration thresholds, intercalation thermodynamics, and perturbation-driven transitions across varied chemistries, the present work extends that foundation into a unified, testable relation. Looking ahead, the CBED rule offers a new and practical screening tool to accelerate experimental discovery while potentially forging a conceptual bridge between real-space energetics and dynamical/kinetic viewpoints that influence superconductivity across diverse mechanisms.

Funding

The National High Magnetic Field Laboratory is supported by the National Science Foundation, United States through NSF/DMR-212-8556, NSF/DMR-1644779, and the State of Florida.

Declaration of competing interest

The authors declare that they have no known competing financial interests or personal relationships that could have appeared to influence the work reported in this paper.

Acknowledgments

The author sincerely thanks A.L. Centers, K. Thirunavukkuarasu, E.S. Choi, M. Lee, S. McGill, K. Wei, M. McFarland, T. Asaba, M. Lee, H. Whitelock, S. Zhang, C. Beekman, J. Jaroszynski, C. Niu, L. W. Nelson, J. Smith, D. Ratkovski, S.A. Maier, C. McNiel, T. Murphy for many useful discussions.

Appendix A. Supplementary data

Supplementary material related to this article can be found online at https://doi.org/10.1016/j.nxmate.2026.102415.

Data availability

All C.I.F. data were obtained from the same open data source location, materialsproject.com [19], and open access articles by Celementi et al [20,21] were referenced for all Z_{eff}.

References

[1] M. Lal, K.M. Gangotri, Innovative study in renewable energy source through mixed surfactant system for eco-friendly environment, Environ. Sci. Pollut. Res. 30 (2023) 98805–98813.
[2] J. Cai, W. Wei, X. Hu, D.A. Wood, Electrical conductivity models in saturated porous media: A review, Earth-Sci. Rev. 171 (2017) 419–433.
[3] C. Korte, J. Keppner, A. Peters, N. Schichtel, H. Aydin, J. Janek, Coherency strain and its effect on ionic conductivity and diffusion in solid electrolytes – an improved model for nanocrystalline thin films and a review of experimental data, Phys. Chem. Chem. Phys. 16 (2014) 24575–24591.
[4] A. Chandra, B. Bagchi, Beyond the classical transport laws of electrochemistry: New microscopic approach to ionic conductance and viscosity, J. Phys. Chem. B 104 (2000) 9067–9080.
[5] A. Davidson, M. Tinkham, Phenomenological equations for the electrical conductivity of microscopically inhomogeneous materials, Phys. Rev. B 13 (1976) 3261–3267.
[6] R. Franz, G. Wiedemann, Ueber die Wärme-Leitungsfähigkeit der metalle, 1853.
[7] Neil W. Ashcroft, Solid state physics, Holt, Rinehart and Winston, 1976.
[8] B.T. Matthias, Empirical relation between superconductivity and the number of valence electrons per atom, Phys. Rev. 97 (1955) 74–76.
[9] B.T. Matthias, J.K. Hulm, A search for new superconducting compounds, Phys. Rev. 87 (1952) 799–806.
[10] B.T. Matthias, Transition temperatures of superconductors, Phys. Rev. 92 (1953) 874–876.
[11] B.T. Matthias, in: C.J. Gorter (Ed.), Progress in Low Temperature Physics, Vol. 2, Elsevier, 1957, pp. 138–150.
[12] B.T. Matthias, T.H. Geballe, V.B. Compton, Superconductivity, Rev. Modern Phys. 35 (1963) 1–22.
[13] F. Fabian von Rohr, M.J. Winiarski, J. Tao, T. Klimczuk, R.J. Cava, Effect of electron count and chemical complexity in the Ta-Nb-Hf-Zr-Ti high-entropy alloy superconductor, Proc. Natl. Acad. Sci. USA 113 (2016) E7144–E7150.
[14] C. Pereti, K. Bernot, T. Guizouarn, F. Laufek, A. Vymazalová, L. Bindi, R. Sessoli, D. Fanelli, From individual elements to macroscopic materials: in search of new superconductors via machine learning, Npj Comput. Mater. 9 (2023) 71.
[15] A. Sanna, T.F.T. Cerqueira, Y.-W. Fang, I. Errea, A. Ludwig, M.A.L. Marques, Prediction of ambient pressure conventional superconductivity above 80 K in hydride compounds, Npj Comput. Mater. 10 (2024) 44.
[16] V. Stanev, C. Oses, A.G. Kusne, E. Rodriguez, J. Paglione, S. Curtarolo, I. Takeuchi, Machine learning modeling of superconducting critical temperature, Npj Comput. Mater. 4 (2018) 1–14.
[17] S.G. Jung, G. Jung, J.M. Cole, Machine-learning predictions of critical temperatures from chemical compositions of superconductors, J. Chem. Inf. Model. 64 (2024) 7349–7375.
[18] R. Ramprasad, R. Batra, G. Pilania, A. Mannodi-Kanakkithodi, C. Kim, Machine learning in materials informatics: recent applications and prospects, Npj Comput. Mater. 3 (2017) 54.
[19] Materials Project. https://next-gen.materialsproject.org/materials/mp-763?formula=MgB2.
[20] E. Clementi, D.L. Raimondi, W.P. Reinhardt, Atomic screening constants from scf functions. II. Atoms with 37 to 86 electrons, J. Chem. Phys. 47 (1967) 1300–1307.
[21] E. Clementi, D.L. Raimondi, Atomic Screening Constants from SCF functions, J. Chem. Phys. 38 (1963) 2686–2689.
[22] C.J. Scott, Rigorous screened interactions for realistic correlated electron systems, Phys. Rev. Lett. (2024) 132.

[23] C. Pellegrini, A. Sanna, Ab initio methods for superconductivity, Nat. Rev. Phys. 6 (2024) 509–523.
[24] T. Wang, Origin of the Coulomb pseudopotential, Phys. Rev. B 107 (2023).
[25] J. Bauer, Retardation effects and the Coulomb pseudopotential in the theory of superconductivity, Phys. Rev. B 87 (2013).
[26] A. Davydov, Ab initio theory of plasmonic superconductivity within the Eliashberg and density-functional formalisms, Phys. Rev. B 102 (2020).
[27] A. Sanna, Combining eliashberg theory with density functional theory for the accurate prediction of superconducting transition temperatures and gap functions, Phys. Rev. Lett. (2020) 125.
[28] S.R. Xie, Y. Quan, A.C. Hire, B. Deng, J.M. DeStefano, I. Salinas, U.S. Shah, L. Fanfarillo, J. Lim, J. Kim, G.R. Stewart, J.J. Hamlin, P.J. Hirschfeld, R.G. Hennig, Machine learning of superconducting critical temperature from Eliashberg theory, Npj Comput. Mater. 8 (2022).
[29] K.-H. Lee, First-principles calculations of the Coulomb pseudopotential u*: Application to Al, Phys. Rev. B 52 (1995) 1425–1428.
[30] S.M. Benjamin, Estimating the single-element concentration of intercalated insulators for the emergence of superconductivity, ACS Phys. Chem. Au 2 (2022) 108–117.
[31] S.M. Benjamin, Intercalate Superconductivity and van der Waals equation, ACS Mater. Au (2) (2022) 436–439.
[32] S.M. Benjamin, Pressurization intercalation, doping, and elements: An empirical study of superconductivity near perturbation onsets, Superconductivity 10 (2024) 100098.
[33] C. Pfleiderer, Superconducting phases of f-electron compounds, Rev. Modern Phys. 81 (2009) 1551–1624.
[34] H. Eyring, The activated complex in chemical reactions, J. Chem. Phys. 3 (1935) 107–115.
[35] T. Hao, Electrical conductivity equations derived with the rate process theory and free volume concept, RSC Adv. 5 (2015) 48133–48146, Publisher: The Royal Society of Chemistry.
[36] T. Hao, Theoretical exploration of external pressure impact on superconducting transition temperatures, Chem. Phys. Lett. 802 (2022) 139792.
[37] T Hao, The empty world – a view from the free volume concept and Eyring's rate process theory, Phys. Chem. Chem. Phys. 26 (2024) 26156–26191, Publisher: The Royal Society of Chemistry.
[38] J.S. Schilling, Studies in superconductivity at extreme pressures, Phys. C: Supercond. Appl. 460-462 (2007) 182–185.